Advances in Science and Technology Research Journal

Advances in Science and Technology Research Journal, 2027, 21(1), 146–156
https://doi.org/10.12913/22998624/231181
ISSN 2299-8624, License CC-BY 4.0

Received: 2026.07.17
Accepted: 2026.11.15
Published: 2026.12.01

The use of digital volume correlation with computed tomography to analyze displacement and wall thickness of multi-operational pressing of cylindrical aluminum extrusions

Damian Bańkowski[1*], Piotr Młynarczyk[1], Tomasz Miłek[1]

[1] Department of Materials Science and Materials Technology, Faculty of Mechatronics and Mechanical Engineering, Kielce University of Technology, al. 1000-lecia P.P. 7, 25-314 Kielce, Poland
* Corresponding author's e-mail: dbankowski@tu.kielce.pl

ABSTRACT

This paper presents the possibility of using computed tomography to determine displacements and stresses during controlled deformation. Tomographic examinations are most often used to assess the quality of castings, welded joints, 3D prints, and electronic systems. These non-destructive tests enable spatial imaging of even the smallest changes in the material, such as cracks, porosity, inclusions, and many other imperfections. Dedicated programs enable precise qualitative analysis, including analysis of porosity, inclusions of other materials, material division, creation of a digital twin, and other advanced options such as digital volume correlation or analysis of the state of displacements and stresses. The digital volume correlation tool allows for the comparison of components in two states before and after deformation. The tests were conducted on aluminum samples. The samples were first extruded and then re-extruded in the next three stages. Single-voxel displacement tracking was used to determine the displacements and von Mises strain in the material. VG Studio software allows for visual representation of displacement and stress. The data obtained also enabled analysis of the thickness of the wall after deformation. The research results indicate that tomographic examinations and digital volume correlation (DVC) assessment can be successfully used to monitor the condition of devices and structures. The scientific aim of the article is to reveal the magnitude of changes in material displacement in extruded elements and compare them with the change in the height of the extrudates. Moreover, the work aims to show changes in the wall thickness of the extrudates throughout their volume and to compare the results of CT tests with measurements using classical methods.

Keywords: computed tomography, digital volume correlation, drawing, material deformation, wall thickness.

INTRODUCTION

Non-destructive testing plays an important role in ensuring the quality and reliability of machines and mechanisms. The most commonly used visual, penetrant or magnetic particle testing methods base their conclusions only on surface analysis [1,2]. The methods that allow for volumetric assessment include ultrasonic, radiographic and tomographic examinations. The main limitation of ultrasonic testing is the need for the tested material to conduct ultrasonic waves. Research using ionizing radiation, X-ray or gamma radiation, enables the study and evaluation of all types of materials. The only limitation that can be encountered is usually the size of the tested element. Moreover, tomographic examinations provide much more information due to the spatial representation of the materials being examined. Classic radiography is ideal for qualitative rather than quantitative assessment and is therefore widely used in industry and medicine – e.g. for precise diagnostics. From an operational perspective, it is crucial to correctly assess any defects and discrepancies, which allows for necessary repairs and replacement of worn components.

This paper presents 3D images of von Mises strain and displacements in cylindrical

cross-sections of aluminum deep drawing obtained using Digital Volume Correlation at limiting drawing ratios without inter-operational annealing, and analysis of wall thicknesses after different stages of deformation. The work visualization of actual changes during subsequent drawing operations and the accompanying displacement and strains and during typical plastic forming processes using digital tomography. Illustrating changes in wall thickness allows for simulating the selection of the appropriate starting material thickness in order to obtain samples with the desired minimum wall thickness. The use of tomographic examinations and digital analyses allows for a full qualitative analysis of actual deformations during plastic processing. The novelty of this work is the tomographic analysis for the tracking of spatial changes, material displacements in all three planes, not just in the extrusion plane as a measurement of redrawing height changes. Furthermore, the tomographic method graphically presents changes in the extrusion wall thickness with high precision. Wall thickness measurements using a micrometer screw typically involve several or a dozen measurements, and achieving a high-resolution thickness map requires a significant amount of work. The research results presented in the paper, using the example of a simple cylindrical part, clearly show the usefulness of the DVC method, which can be used to analyze parts with more complex shapes and geometries.

Computed tomography

Radiographic imaging uses X-rays that pass through the object being examined. While radiography takes an X-ray image from a single angle, in computed tomography (CT) the object is scanned from multiple angles [3,4] typically from about several hundred to several thousand. The set of projections is then used to reconstruct a high-resolution three-dimensional image of the object [5,6].

Computed tomography is one of the most important methods of imaging the interior of objects without the need to destroy them [7]. This technique is based on the reconstruction of a three-dimensional image of the material or element being examined based on a series of projections recorded from different angles. The most commonly used variety is X-ray computed tomography (XCT or μCT), which is widely used in materials engineering, biomechanics, medicine and research on composite structures. Tomographic examinations are used for the analysis of castings [8], including porosity analyses [9], for testing composites such as concretes [9,10], the quality of welds [11], additive manufacturing methods, 3D printing [12], or for medical applications for the observation of living organisms [13]. Of particular importance is the ability to obtain spatial information about the geometry and microstructure of the examined object, which is a significant advantage over classical two-dimensional RT techniques.

The basis of X-ray tomography is the phenomenon of weakening of X-rays when passing through a material. The attenuated radiation is measured by a detector, creating a two-dimensional projection of the object (X-ray image) [5]. The degree of absorption depends on the density and chemical composition of the object being examined. The recorded projections are then processed using reconstruction algorithms, such as the filtered inverse Radon transform or iterative methods, to produce a digital volumetric model composed of voxels, the three-dimensional equivalent of pixels [14].

The development of digital tomography has enabled the analysis of the internal structure of materials with very high spatial resolution, reaching even single micrometers in the case of microtomography. This made it possible to study porosity, crack initiation, damage propagation and microstructural changes occurring under the influence of mechanical loads or technological processes. Modern tomographic systems also allow for in situ testing [3, 15], during which the sample is subjected to loading directly scanning.

Digital volume correlation

Digital volume correlation (DVC) is a three-dimensional extension of the digital image correlation (DIC) method known since 1999 [16, 17]. DVC uses naturally occurring image textures to track displacements [17]. This technique is used to determine displacement [18] and strain fields within a material based on the analysis of successive tomographic images obtained before and after deformation of the sample. The DVC method enables non-contact and non-destructive measurement of internal deformations, which makes it particularly useful in the study of heterogeneous materials [19] and structures with complex geometry.

Accurate measurements of three-dimensional strains in materials are a challenge in modern research on the mechanical properties of materials. Unlike classical measurements based mainly on measuring surface deformations, the method using computed tomography enables the analysis of internal changes. CT therefore provides valuable information for materials with complex geometries, composites, or porosities. A novel physics-based deep learning (DVC) solution for DVC (PiNetDVC) [20] was developed by Wang et al. In this approach, strain is treated as a direct output of the network. Consistency between the strain and displacement fields is enforced through a comparison of the network-generated strains and the strains obtained from displacement-gradient calculations [20].

The basic principle of DVC operation is to track changes in the position of characteristic microstructure fragments between the reference image and the image after deformation [21-24]. The image volume is divided into smaller subareas called subvolumes, for which a correlation function is determined, defining the degree of similarity between corresponding image fragments. Maximizing the correlation coefficient allows the determination of local voxel displacements and subsequent calculation of strain fields.

The literature distinguishes two basic approaches to the implementation of DVC algorithms: local and global methods. Local methods analyze each subvolume independently, which provides great computational flexibility, but may lead to greater sensitivity to image noise. Global methods, on the other hand, use continuous functions to approximate the displacement field, often based on the finite element method (FEM), which allows for smoother and more stable results.

One of the key limitations of the DVC technique is the quality of tomographic images. The measurement accuracy depends on the scanning resolution, noise level, microstructure contrast and the stability of the tomographic system [25,26]. Unlike classical DIC, DVC does not allow for the creation of an artificial random pattern inside the material, therefore the method is based on the natural microstructural features of the tested object.

The dynamic development of imaging techniques and the increase in computer processing power have contributed to a significant increase in the applications of DVC. This method is currently used in bone and soft tissue biomechanics, composite materials research, crack propagation analysis, soil mechanics, and quality control of additively manufactured components [27,28]. Algorithms using artificial intelligence and machine learning are also increasingly being developed to improve the speed and accuracy of volumetric data analysis.

The combination of computed tomography with the Digital Volume Correlation method enables comprehensive analysis of the behavior of materials under real load conditions. Due to its ability to determine full three-dimensional displacement and strain fields, this technique is currently one of the most important tools in experimental mechanics of materials.

MATERIAL AND METHODS

The tests were performed on sheets of nominal thickness 1 mm made of EN-AW 1050A aluminum alloy with the chemical composition as in Table 1. EN-AW 1050A alloy is technically pure aluminum, minimum 99.5% purity, characterized by excellent corrosion resistance and very good thermal and electrical conductivity [29].

In order to determine the mechanical properties, samples -without heat treatment, were prepared for a static tensile test. Tensile and drawing tests were carried out at a temperature of 23.5 degrees Celsius. The average thickness a_0 and width b_0 of the samples determined on the basis of three measurements with a micrometer screw are presented in Table 2 together with the calculated cross-sections S_0 and the determined average values of the maximum forces F_m obtained in the static tensile test.

The static tensile test was performed on a *LabTest 5.20SP1* testing machine (with a maximum load of 20 kN) equipped with *Test&Motion* software. The press meets 0.5 metrological class requirements for force and displacement measurements. The testing machine was manufactured by LABORTECH company (Opava, the Czech Republic). Three measurements of samples were performed and the average results are presented in Table 3.

The changes in tensile force and displacement obtained for selected samples were converted into stress versus relative strain graphs which are presented in Figure 1 and 2, respectively.

The multi-operation deep drawing process was performed using laboratory press-forming dies mounted on a *LabTest 5.20SP1* testing

Table 1. Chemical composition of the EN-AW 1050A aluminum alloy, wt. %

Al	Fe	Si	Zn	Ti	Mg	Mn	Cu
min. 99.50	max. 0.40	max. 0.25	max. 0.07	max. 0.05	max. 0.05	max. 0.05	max 0.03

Table 2. Dimensions and maximum values of forces obtained in static tensile test

Material	a_0 (mm)	b_0 (mm)	S_0 (mm²)	F_m (N)
EN-AW 1050A aluminum	0.970	12.49	12.12	1731.60
	0.960	12.48	11.98	1772.80
	0.970	12.45	12.08	1754.74

Table 3. Mechanical properties of materials used in the deep drawing process

Material	R_m (MPa)	$R_{p0.2}$ (MPa)	A (%)	$A_{11.3}$ (%)
EN-AW 1050A	145.37	129.75	18.97	13.5

machine. During the tests, force and displacement results were recorded using *Test&Motion* software. The design of the tooling is shown in Figure 3. Table 4 presents the dimensions of the most important elements (punches and dies) included in it [30]. The following notations were adopted in the table: d_s and d_m – diameters of the punch and the die; r_s and r_m – radius of the die and the punch, respectively. To prevent the flange folding, a blank holder was used in the first operation (element no. 3 in Figure 3).

For the deep drawing tests, blanks were prepared which were cut from aluminum sheet belts on a blanking die mounted on a Bussmann press with a maximum load of 1 MN. The experimental investigations were conducted for discs with a diameter of d_0 = 66 mm and a thickness of g_0 = 1 mm (which corresponded to the relative thickness of 0.015).

RESULTS OF EXPERIMENTAL INVESTIGATIONS

The experimental results of multi-operation deep drawing tests were cylindrical draw pieces, the dimensions of which, along with the calculated drawing coefficients and relative deformations, are presented in Table 5. The following notations are used in the table: $m_{1..n}$ – drawing coefficients, D_{CT} – outer diameter of the draw-piece from CT measurements, g- wall thickness in the middle of

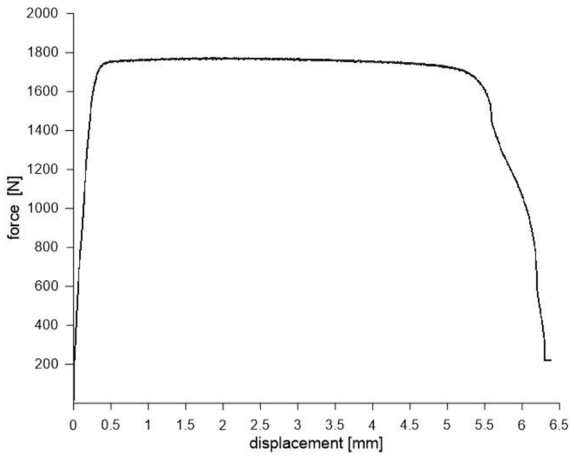


Figure 1. The force vs. displacement for aluminum in static tensile test

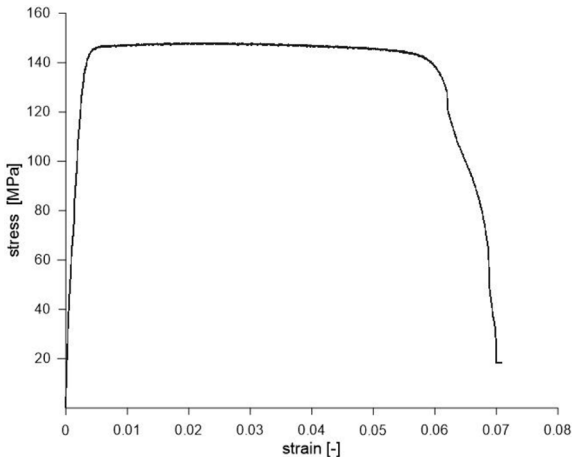


Figure 2. The stress vs. relative strain for aluminum after static tensile test

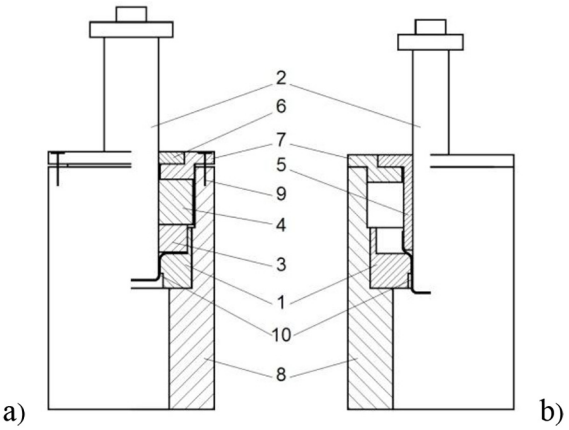


Figure 3. Laboratory press-forming dies for first draw in deep drawing (a) and redrawing (b) of cylindrical draw piece, where: 1 – die; 2 – punch; 3 – blank-holder; 4 – ring, 5 – pilot sleeve, 6 – adjusting ring, 7 – cover of die holder, 8 – die holder, 9 – set screws, 10 – draw piece

the draw-piece height, h- minimum value of the draw-piece height, ε_c – relative strain.

The drawing coefficient $m_{1..n}$ in several operations was calculated using formula (1) [31,32]:

$$m_{1..n} = \frac{d_n}{d_{n-1}} \tag{1}$$

where: d_n – post-operation draw piece diameter measured at half of the wall thickness; (mm), d_{n-1} – pre-operation material diameter (blank or draw piece).

The relative unit strain ε_c was calculated using the formula [31,32]:

$$\varepsilon_c = (1 - m_1 \cdot m_2 \ldots \cdot m_n) \cdot 100\% \tag{2}$$

The lowest drawing ratio *m* (and therefore the highest degree of deformation – strain factor ε_c) was adopted in the first operation (single drawing). In subsequent operations, *m* was increased and ε_c was decreased. Inter-operational annealing was not used between operations because the deformation ε_c was less than the limit deformation for aluminum. Examples of draw pieces obtained in the tests are shown in Figure 4.

During the tests, changes in drawing forces were recorded as a function of punch displacement. These changes are presented for each operation in Figure 5.

The punch displacement at which the forces reached their maximum value relative to the total deep drawing distance was 0.35 for the first drawing operation (single drawing); 0.5 for the second operation (first redrawing), 0.6 for the third operation (second redrawing), and 0.75 for the fourth operation (third redrawing). The highest maximum force was achieved in the first operation, reaching 10.8 kN. In subsequent operations, the maximum values decreased, reaching 8.2 kN, 5.3 kN and 4.1 kN, respectively. It is worth noting that the force values decreased despite the progressive hardening of the material. This is due to the assumed strain in each operation. In the first operation, the unit strain exceeded 44%, while in the subsequent operations, it decreased to 24%, 20%, and in the final operation, to 19%, respectively. The adoption of decreasing degrees of deformation in subsequent operations is typical for various metal forming technologies [1,32], especially in stamping technologies [30,31,33].

Table 4. Dimensions of punches and dies used in the experiments

Parameter	Single drawing	First redrawing	Second redrawing	Third redrawing
d_s	35.5	26.5	21.5	17.5
d_m	38	29	24	20
r_s	5	3	3	3
r_m	5	3	3	3

Table 5. Sample dimensions obtained from tests

Parameter	$m_{1..n}$	D_{CT} (mm)	g (mm)	h_{mm} (mm)	ε_{total} (%)
Single drawing	0.556	37.83	1.03	20.62	44.4
First redrawing	0.766	28.96	0.94	32.66	57.41
Second redrawing	0.829	24.01	0.95	39.55	64.69
Third redrawing	0.821	19.72	0.95	49.55	71.01



Figure 4. Individual stages of forming the draw pieces in four operations from a blank at $s_0/D=0.015$

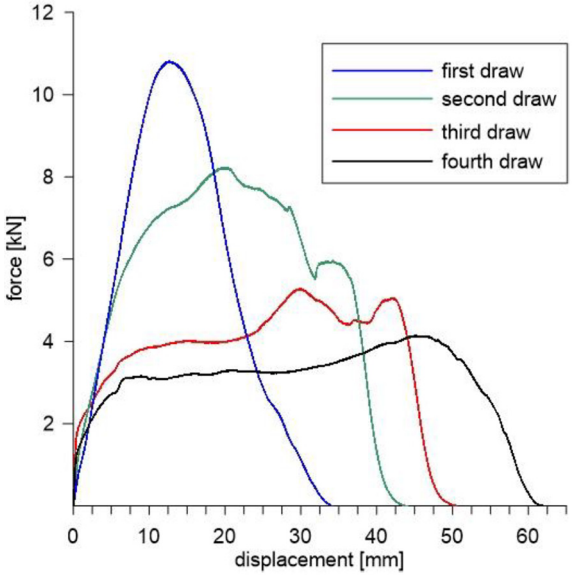


Figure 5. The force vs. displacement obtained for deep drawing (first draw) and redrawing (second, third and fourth draw) tests in experiment

CT SCANNING PROCEDURE

Computed tomography (CT) scans were conducted using a NIKON M2 LES SYSTEM scanner equipped with a 450 kV microfocus X-ray source, shown in Figure 6. Image acquisition was performed with a VAREX XRD 1611 XP flat-panel detector featuring a resolution of 4048 × 4048 pixels and a pixel pitch of 0.1 mm. The detailed exposure settings are listed in Table 6. Reconstruction of the tomographic datasets was carried out using Inspect-X software (Version 6.8, Nikon Metrology). Subsequent visualization of cross-sectional images, quantitative analyses, defect observations, wall thickness measurements, and digital volume correlation (DVC) evaluations were performed in VGSTUDIO MAX 2022.4 (Volume Graphics).

The tomographic examination of a single sample was performed in approximately 16 minutes, with the ambient temperature maintained at 18 °C.

IMAGE PROCESSING AND DVC ANALYSIS

The acquired two-dimensional radiographic projections were reconstructed into three-dimensional volumetric datasets using Inspect-X software (Version 6.8, Nikon Metrology). Subsequent examination of the reconstructed volumes, including cross-sectional visualization, quantitative analysis and wall thickness measurements was carried out in VGSTUDIO MAX 2022.4 (Volume Graphics). The same software was also employed to perform DVC analyses.

Digital Volume Correlation is an advanced image-analysis technique integrated into VGSTUDIO MAX that enables the evaluation of internal displacements by comparing volumetric datasets acquired before and after deformation. The method tracks the movement of individual voxels between reference and deformed states, making it suitable for the assessment of in-situ experiments and structural changes under applied loading conditions. In addition to determining local displacement fields and strain tensors, the software provides graphical representations of material deformation through vector arrows and displacement trajectories. Furthermore, the obtained results can be transferred to finite element (FE) models, facilitating the validation and comparison of numerical simulations with experimentally measured behavior [34].

The study compared tomographic reconstructions of samples after subsequent stages of extrusion to the pre-deformation state. The tests were performed on the same sample, successively by performing plastic processing and CT reconstruction. In this way, the process of first pressing to extrusion, the process of the second pressing to the first pressing and the process of the third pressing to the second pressing were analyzed.

Following reconstruction, the 3D volumetric models were processed using DVC analysis. The method made it possible to identify and visually

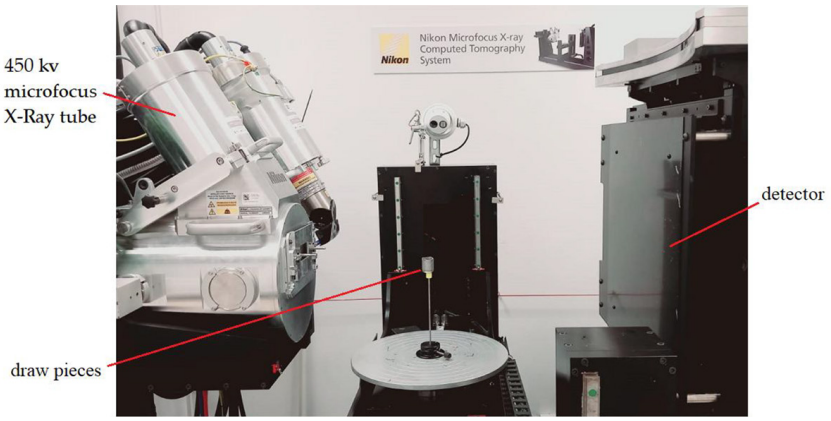


Figure 6. Image of the NIKON M2 LES System computed tomography scanner used during the examination of the test specimen

Table 6. X-ray acquisition parameters

Parameter	Value
Voltage	300 kV
Current	200 µA
Power	60.0 W
Filter	No
Voxel size	25.01 µm
Projection	2600
Time per projection	354 ms
Distance source-sample	254.74 mm
Distance source-detector	1018.29 mm

map deformation patterns in the draw piece, providing insight into material displacements and structural changes induced by the preceding drawing process.

The DVC evaluation was carried out ex situ using the complete specimen volume. The undeformed drawpiece was designated as the reference dataset, while the volumes obtained after each successive drawing stage were compared against this initial state. Prior to the correlation analysis, the datasets were spatially aligned using a best-fit registration procedure.

The DVC computations were performed using the original CT reconstruction resolution without any resampling, corresponding to a voxel size of 25 µm. A local non-linear transformation model was applied to capture the deformation behavior. In this approach, deformation is represented by a spatially varying displacement field defined by displacement vectors distributed over a regular grid of control points. The displacement field between neighboring control points was interpolated using cubic B-spline functions. A control-point spacing of 0.4 was selected, equivalent to 16 voxels. Similarity between the reference and deformed volumes was evaluated using the normalized cross-correlation criterion. The optimization process was performed with a maximum of 500 iterations.

Figure 7 shows the displacement magnitude and Von Mises strain comparing the digital tomographic models of the sample after the first deep drawing with the sample after re-extrusion. Similarly, Figure 8 is a comparison of the second pressing operation compared to the first pressing operation. Figure 9 is a digital volume correlation analysis of the third drawing operation to the second drawing operation. Each semi-transparent drawing in Figures 7 to 9a) represents the initial reference state to which the post-deformation state was compared – the colored drawing.

Based on tomographic examinations of the extrudates after subsequent extrusion and embossing operations, it was possible to perform digital volume correlation analysis. VGStudio software enables tracking of individual voxel displacements. Based on the displacement magnitude analysis in Figures 7–9 a), it can be seen that the displacements are not uniform throughout the volume. The analyses show that the largest voxel displacements occur in the upper parts of the extrusions. The lower part of the extrusion, encompassing the bottom, exhibited the smallest material displacement. The largest displacement magnitude was achieved as a result of the first extrusion operation, reaching of 13.4 mm. However, as can be read from Table 5, the increase in the height of the extrusion after the first redrawing reached almost 12 mm. The second redrawing operation showed a CT displacement magnitude

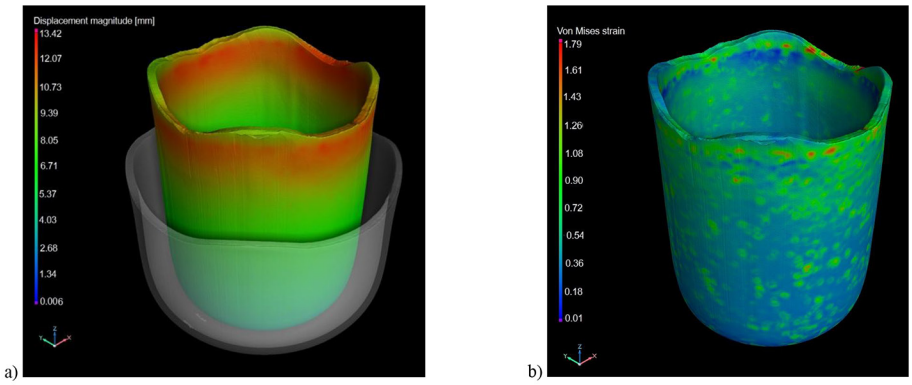


Figure 7. Visualization of a) displacement magnitude and b) Von Mises strain after the first extrusion operation

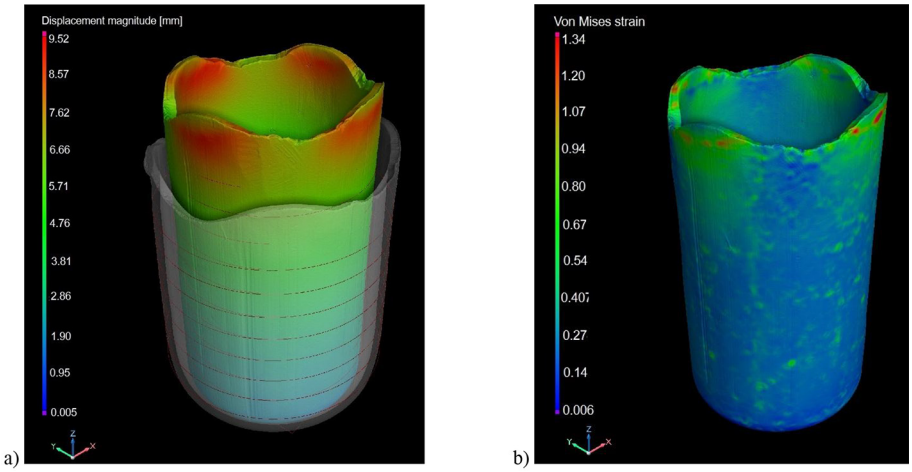


Figure 8. Visualization of a) displacement magnitude and b) Von Mises strain after the second pressing operation

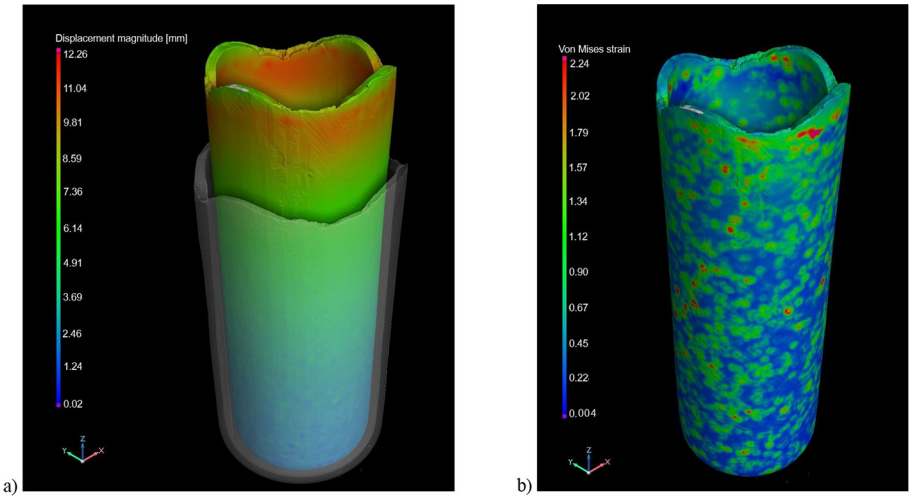


Figure 9. Visualization of a) displacement magnitude and b) Von Mises strain after the third pressing operation

of 9.5 mm, and the third 12.2 mm. Based on Table 5, the increase in the extrusion height reached almost 7 mm after the second redrawing and 10 mm after the third redrawing. It can be concluded that the deformation obtained from computed tomography reach values approximately 2 mm greater than the observed changes in the relative height of the extrudates. This may be due to the

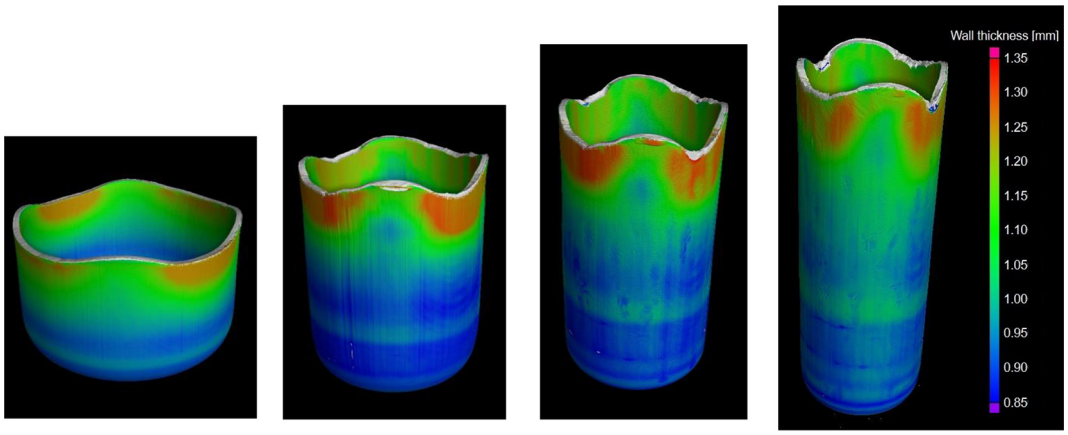


Figure 10. Analysis of wall thickness of draw pieces in four operations

high accuracy of the tomographic method and the fact that changes in all planes are taken into account. Height measurements with a caliper are based on recording deformation changes only in one plane - the extrusion or redrawing plane.

The distribution of predicted Von Mises strain is similar to observe deformations. The lowest Von Mises strain occur in the lower parts of the stamps, and the highest in the upper parts. However, as can be seen after subsequent stamping operations, especially the sample in Figure 9 b), after the third stamping, has red dots of high Von Mises strain along the entire length of the cylindrical section.

Additionally, VGStudio software allows for wall thickness analysis. As constraints, material with a thickness of 0.85 mm to 1.35 mm was analyzed. Graphical visualizations of wall thickness distributions are presented in Figure 10.

Based on the wall thickness analyses performed, key information on the course of plastic deformation between subsequent pressing operations can be obtained. The nominal thickness of the sample per extrusion was 1 mm. As can be seen in Figure 10a), the first operation causes slight changes in the extrusion thickness. Imaging obtained from computed tomography shows that in the lower part of the extrusion the wall thickness is thinned to approximately 0.9 mm, while in the upper part the wall thickness increases to up to 1.3 mm, which is an increase in thickness of up to 30%. By examining the upper part of the extrudates, it can be seen that the extrusion and redrawing processes result in significant differences in wall thickness. After each stage of plastic forming, four peaks and four valleys can be distinguished in the samples, arranged symmetrically at approximately 90 degrees to the sample axis. The most axially stretched parts of the side wall are approximately 0.2 mm thinner than the parts with the smallest axial deformation – the depressions visible on the extrusions. Comparing the wall thickness results from tomographic examinations to measurements made using a micrometer screw (Table 5) shows a high degree of agreement between the measurements near the bottom and up to approximately half the height of the extrusions. The upper fragments of the extrudates from CT measurements are 0.1 mm to even 0.3 mm thicker than the results from measurements made with classic tools. Furthermore, graphical results from tomographic studies show that the quality and wear of plastic forming tools are of great importance. Any wear on the surfaces of dies and punches will result in defects being mapped onto the extruded parts.

CONCLUSIONS

DVC made it possible to understand the changes related to the displacement and stress of the material that occur between subsequent extrusion and redrawing operations.

Based on the DVC analysis, the largest material displacements during extrusion occur in the upper parts of the extrusions and the smallest in the bottom area.

The displacements obtained from computed tomography reach values approximately 2 mm greater than the changes in the relative height of the extrudates made and read using a caliper. These differences may be due to the fact that the tomographic method measures the sample

deformation in all three planes, while in one plane only the change in the sample height is measured.

Digital analysis of tomographic reconstructions shows that as a result of extrusion and redrawing, the obtained samples do not have the same wall thickness. After the extrusion and redrawing process, the wall is thinned by approximately 0.1 mm near the bottom, from a dimension close to the nominal thickness in the middle to a thickening by up to 0.3 mm in the upper part of the samples.

It should be noted that the increase in thickness in the upper part of the samples is not uniform around the circumference. The largest peaks in the cylindrical portion of the samples are characterized by significantly thinner walls than the adjacent valleys. The recorded thickness difference reaches approximately 0.3 mm.

The wall thicknesses of the lower parts of the extrusions, both measured with a caliper and from computed tomography, are consistent. However, the upper parts of the extrusions are characterized by a thickness of approximately 0.1 to 0.3 mm greater in the case of tomographic examinations than in classical measurements.

REFERENCES

1. Gronostajski Z., Pater Z., Madej L., Gontarz A., Lisiecki L., Łukaszek-Sołek A., Łuksza J., Mróz S., Muskalski Z., Muzykiewicz W., Pietrzyk M., Śliwa R. E. Tomczak, J. Wiewiórowska S., Winiarski G., Zasadziński J.,Ziółkiewicz S. Recent development trends in metal forming. Archives of Civil and Mechanical Engineering 2019, 19(3): 898–941.
2. Bańkowski D., Młynarczyk P. Visual testing of castings defects after vibratory machining. Archives of Foundry Engineering. 2020, 4: 72–7, https://doi.org/10.24425/afe.2020.133350
3. Köhler, D., Kupfer, R., Troschitz, J., Gude, M. In Situ Computed Tomography—Analysis of a Single-Lap Shear Test with Clinch Points. Materials 2021, 14: 1859. https://doi.org/10.3390/ma14081859
4. Depczynski W. P., Bankowski D., Mlynarczyk P. S. Computed tomography and scanning electron microscopy analysis of a friction stir welded Al-Cu joint. Archives Of Foundry Engineering. 2023, 23(4): 5–71. https://doi.org/10.24425/afe.2023.146680
5. Carmignato, S., Dewulf, W., Leach, R. Industrial X-ray Computed Tomography; Springer International Publishing: Cham, UK, 2018.
6. Bańkowski, D., Nowakowski, Ł., Skrzyniarz, M., Błasiak, S., Kurp, P., Depczyński, W. P., Młynarczyk, P. S. Evaluating the impact of the tool and additional fruit cutting on changes of pitted cherries using digital volume correlation with computed tomography. Advances in Science and Technology Research Journal, 2025, 19(11): 162–175. https://doi.org/10.12913/22998624/209179
7. Żaba, K., Gracz, D., Trzepieciński, T., Książek, M., Sitek, R., Tchórz, A., Balcerzak, M., Wałach, D. Application of x-ray computed tomography to identify defects in lost wax ceramic moulds for precision casting of turbine blades. Materials 2024, 17: 5088. https://doi.org/10.3390/ma17205088
8. Cunningham, R., Narra, S.P., Montgomery, C., Beuth, J., Rollett, A.D. Synchrotron-based X-ray microtomography characterization of the effect of processing variables on porosity formation in laser power-bed additive manufacturing of Ti-6Al-4V. JOM 2017, 69: 479–484.
9. Kaczmarczyk, G.P., Kinasz, R., Bilozir, V., Bidenko, I. Application of x-ray computed tomography to verify bond failures mechanism of fiber-reinforced fine-grain concrete. Materials 2022, 15: 2193. https://doi.org/10.3390/ma15062193
10. Skarzynski, L. Suchorzewski, J. Mechanical and fracture properties of concrete reinforced with recycled and industrial steel fibers using Digital Image Correlation technique and X-ray micro computed tomography. Construction and Building Materials. 2018, 183: 283–299. https://doi.org/10.1016/j.conbuildmat.2018.06.182
11. Teichmann F, Ziemer A, Leitner M, Hensel J, Dilger K. Linear elastic FE-analysis of porous, laser welded, heat treatable, aluminium high pressure die castings based on x-ray computed tomography data. Materials. 2020, 13(6): 1420. https://doi.org/10.3390/ma13061420
12. Megersa, G.K., Sitek, W., Nowak, A.J., Krzemiński, Ł., Kajzer, W., Niewolik, D. Impact of layer thickness on mechanical properties and surface roughness of FDM-printed carbon fiber-PEEK composite. Materials. 2026, 19(9):1692. https://doi.org/10.3390/ma19091692
13. Bartkowiak T, Madalińska D, Mietliński P, Kaczmarek J, Gapiński B, Pelic M, Paczos P. Quantification of Thread Engagement in Screw-Plate Interface of Polyaxial Locking System Using X-ray Computed Tomography. Materials. 2023; 16(17):5926. https://doi.org/10.3390/ma16175926
14. Carmignato, S., Dewulf, W., Leach, R. Industrial X-ray Computed Tomography; Springer International Publishing: Cham, UK, 2018.
15. Bańkowski D., Młynarczyk P., Spadło S., Sójka R., Klamczyński K. Tomographic testing of alnico alloys. Proceedings 31 International Conference on Metallurgy and Materials. 2022; 675–681, https://doi.org/10.37904/metal.2022.4507

16. Kunz H, Stammen E, Dilger K. Local displacement measurements within adhesives using particle tracking and in-situ computed tomography. J Adhes 2017; 93: 531–549.
17. Yang, J., Hazlett, L., Landauer, A. et al. Augmented Lagrangian Digital Volume Correlation (ALDVC). Exp Mech 2020, 60: 1205–1223. https://doi.org/10.1007/s11340-020-00607-3
18. Bay B.K. Methods and applications of digital volume correlation, J. Strain Anal. Eng. Des. 2008, 43(8): 745–760A.
19. Sun X., Lukić B., Chen Y., Xu Z., Chapman D., Eakins D. 3D micro-mechanics of a CFRP laminate under high-rate and varying temperature loading using digital volume correlation, Composites Part B: Engineering, 2026, 321: 113693, https://doi.org/10.1016/j.compositesb.2026.113693
20. Madi S. E., Chatziathanasiou T., Wevers M., Swolfs Y., Soete J. Composites in biaxial cruciform tests: effect of geometry on volumetric strain evolution using X-ray computed tomography and digital volume correlation, Composites Part B: Engineering, 2026, 322: 113744. https://doi.org/10.1016/j.compositesb.2026.113744
21. Wang Z., Zhou H., Liu H. Physics-informed neural networks based digital volume correlation for displacement and strain measurements, Mechanical Systems and Signal Processing, 2026, 248: 113998. https://doi.org/10.1016/j.ymssp.2026.113998
22. Pan B., Wang B. Some recent advances in digital volume correlation, Optics and Lasers in Engineering. 2020, 135: 106189. https://doi.org/10.1016/j.optlaseng.2020.106189
23. Holmes J., Sommacal S., Das R., Stachurski Z., Compston P. Digital image and volume correlation for deformation and damage characterisation of fibre-reinforced composites: A review, Composite Structures, 2023.
24. Roberts B.C., Perilli E., Reynolds K.J. Application of the digital volume correlation technique for the measurement of displacement and strain fields in bone: A literature review. Journal of Biomechanics. 2014, 47(5): 923–934. https://doi.org/10.1016/j.jbiomech.2014.01.001
25. Sun X., Lukić B., Chen Y., Xu Z., Chapman D., Eakins D. 3D micro-mechanics of a CFRP laminate under high-rate and varying temperature loading using digital volume correlation, Composites Part B: Engineering, 2026, 321: 113693. https://doi.org/10.1016/j.compositesb.2026.113693
26. Skarzynski L. Suchorzewski J. Mechanical and fracture properties of concrete reinforced with recycled and industrial steel fibers using Digital Image Correlation technique and X-ray micro computed tomography. Construction and Building Materials. 2018, 183: 283–299. https://doi.org/10.1016/j.conbuildmat.2018.06.182
27. Megersa G.K., Sitek W., Nowak A.J., Krzemiński Ł., Kajzer W., Niewolik D. Impact of layer thickness on mechanical properties and surface roughness of FDM-printed carbon fiber-PEEK composite. Materials. 2026; 19(9): 1692. https://doi.org/10.3390/ma19091692
28. Bartkowiak T., Madalińska D., Mietliński P., Kaczmarek J., Gapiński B., Pelic M., Paczos P. Quantification of thread engagement in screw-plate interface of polyaxial locking system using x-ray computed tomography. Materials. 2023, 16(17): 5926. https://doi.org/10.3390/ma16175926
29. Madi S.E., Chatziathanasiou T., Wevers M., Swolfs Y., Soete J. Composites in biaxial cruciform tests: effect of geometry on volumetric strain evolution using X-ray computed tomography and digital volume correlation, Composites Part B: Engineering, 2026, 322: 113744. https://doi.org/10.1016/j.compositesb.2026.113744
30. Bańkowski, D., Spadło, S. Influence of the smoothing conditions in vibro-abrasive finishing and deburring process for geometric structure of the surface machine parts made of aluminum alloys EN AW-2017A. In Proceedings of 24th International Conference on Metallurgy and Materials METAL; Tanger Ltd.: Ostrava, Czech Republic, 2015; 1062–1068.
31. Miłek T. Evaluation of the possibility of deep drawing of aluminium cylindrical drawpieces from sheets at different relative rolling reductions. Journal of Physics: Conference Series 2021, 1736: 1–8.
32. Pacanowski J. Design of deep drawing process of axisymmetric draw pieces and design press-forming dies T1 Methods and directives for deep drawing of axisymmetric draw pieces (Kielce: Kielce University of Technology), chapter 4.7 2018, 125–138 (in Polish).
33. Lange K. Handbook of metal forming. McGraw-Hill Book Company, chapter 22 1985, 22.1–22.10.
34. Winiarski, G., Bulzak, T. A., Wójcik, Ł. Szala, M. Numerical analysis of a six stage forging process for producing hollow flanged parts from tubular blanks. Advances in Science and Technology Research Journal 2020, 14(1): 201–208. https://doi.org/10.12913/22998624/116748
35. https://volumegraphics.hexagon.com/en/products/add-on-modules/digital-volume-correlation.html